3D Organotypic Spinal Cultures: Exploring Neuron and Neuroglia Responses upon Prolonged Exposure to Graphene Oxide

Rossana Rauti[1], Mattia Musto[1], Neus Lozano[2], Elena Bonechi[3], Clara Ballerini[4*], Kostas Kostarelos[2*], Laura Ballerini[1*]

[1]Scuola Internazionale Superiore di Studi Avanzati (SISSA), Italy, [2]Nanomedicine Lab, Faculty of Biology, Medicine & Health and National Graphene Institute, AV Hill Building, University of Manchester, Manchester, United Kingdom, United Kingdom, [3]Department NEUROFARBA, University of Florence, 50139 Florence, Italy, Italy, [4]Laboratory of Neuroimmunology, Dipartimento di Medicina Sperimentale e Clinica, University of Firenze, Firenze, Italy, Italy

Submitted to Journal:
Frontiers in Systems Neuroscience

Article type:
Original Research Article

Manuscript ID:
429246

Received on:
05 Oct 2018

Revised on:
06 Dec 2018

Frontiers website link:
www.frontiersin.org

Conflict of interest statement

The authors declare that the research was conducted in the absence of any commercial or financial relationships that could be construed as a potential conflict of interest

Author contribution statement

M.M. and R.R. performed all cell biology, electrophysiology, and confocal experiments and analysis; N.L. and K.K. contributed to the synthesis and characterization of thin graphene oxide (s-GO); E.B. and C.B. designed and performed the supernatant measures; C.B. and L.B. conceived the study and the experimental design; C.B., R.R. and L.B. wrote the manuscript.

Keywords

Graphene, organotypic cultures, patch-clamp, Microglia, Microvesicles

Abstract

Word count: 245

Graphene-based nanomaterials are increasingly engineered as components of biosensors, interfaces or drug delivery platforms in neuro-repair strategies. In these developments, the mostly used derivative of graphene is graphene oxide. To tailor the safe development of graphene oxide nanosheets, we need to model in vitro tissue responses, and in particular the reactivity of microglia, a sub-population of neuroglia that acts as the first active immune response, when challenged by graphene oxide. Here, we investigated central nervous system tissue reactivity upon long-term exposure to graphene oxide nanosheets in 3D culture models. We used the mouse organotypic spinal cord cultures, ideally suited for studying long-term interference with cues delivered at controlled times and concentrations. In cultured spinal segments, the normal presence, distribution and maturation of anatomically distinct classes of neurons and resident neuroglial cells are preserved. Organotypic explants were developed for two weeks embedded in fibrin glue alone or presenting graphene oxide nanosheets at 10, 25 and 50 µg/mL. We addressed the impact of such treatments on premotor synaptic activity monitored by patch clamp recordings of ventral interneurons. We investigated by immunofluorescence and confocal microscopy the accompanying glial responses to graphene oxide exposure, focusing on resident microglia, tested in organotypic spinal slices and in isolated neuroglia cultures. Our results suggest that microglia reactivity to accumulation of graphene oxide flakes, maybe due to active phagocytosis, may trimm down synaptic activity, although in the absence of an effective activation of inflammatory response and in the absence of neuronal cell death.

Funding statement

We acknowledged financial support from the European Union's Horizon 2020 research and innovation programme under grant agreement No. 696656 and No. 785219 Graphene Flagship

Ethics statements

(Authors are required to state the ethical considerations of their study in the manuscript, including for cases where the study was exempt from ethical approval procedures)

Does the study presented in the manuscript involve human or animal subjects: Yes

Please provide the complete ethics statement for your manuscript. Note that the statement will be directly added to the manuscript file for peer-review, and should include the following information:

- Full name of the ethics committee that approved the study
- Consent procedure used for human participants or for animal owners
- Any additional considerations of the study in cases where vulnerable populations were involved, for example minors, persons with disabilities or endangered animal species

As per the Frontiers authors guidelines, you are required to use the following format for statements involving human subjects: This study was carried out in accordance with the recommendations of [name of guidelines], [name of committee]. The protocol was approved by the [name of committee]. All subjects gave written informed consent in accordance with the Declaration of

Helsinki.
For statements involving animal subjects, please use:
This study was carried out in accordance with the recommendations of 'name of guidelines, name of committee'. The protocol was approved by the 'name of committee'.

If the study was exempt from one or more of the above requirements, please provide a statement with the reason for the exemption(s).
Ensure that your statement is phrased in a complete way, with clear and concise sentences.
All experiments were performed in accordance with the EU guidelines (2010/63/UE) and Italian law (decree 26/14) and were approved by the local authority veterinary service and by our institution (SISSA-ISAS) ethical committee. All efforts were made to minimize animal suffering and to reduce the number of animal used. Animal use was approved by the Italian Ministry of Health, in agreement with the EU Recommendation 2007/526/CE.

Data availability statement

Generated Statement: The datasets generated for this study are available on request to the corresponding author.

frontiers

Manuscript ID: 429246-R1

3D Organotypic Spinal Cultures: Exploring Neuron and Neuroglia Responses upon Prolonged Exposure to Graphene Oxide

Mattia Musto[1a], Rossana Rauti[1a], Artur Filipe Rodrigues[2], Elena Bonechi[3], Clara Ballerini[4*], Kostas Kostarelos[2*], Laura Ballerini[1*]

[1] Neuron Physiology and Technology Lab, International School for Advanced Studies (SISSA), Trieste, Italy
[2] Nanomedicine Lab, Faculty of Biology, Medicine & Health and National Graphene Institute, AV Hill Building, University of Manchester, Manchester, United Kingdom
[3] Department NEUROFARBA, University of Florence, 50139 Florence, Italy
[4] Laboratory of Neuroimmunology, Dipartimento di Medicina Sperimentale e Clinica, University of Firenze, Firenze, Italy

[a] These authors equally contributed to the work

Correspondence:

E-mail: laura.ballerini@sissa.it, clara.ballerini@unifi.it and kostas.kostarelos@manchester.ac.uk

Keywords: graphene oxide, organotypic cultures, patch-clamp, microglia, microvesicles

Number of words: 6809

Number of figures: 5 + 3 Supplemetary

Abstract

Graphene-based nanomaterials are increasingly engineered as components of biosensors, interfaces or drug delivery platforms in neuro-repair strategies. In these developments, the mostly used derivative of graphene is graphene oxide. To tailor the safe development of graphene oxide nanosheets, we need to model *in vitro* tissue responses, and in particular the reactivity of microglia, a sub-population of neuroglia that acts as the first active immune response, when challenged by graphene oxide. Here, we investigated central nervous system tissue reactivity upon long-term exposure to graphene oxide nanosheets in 3D culture models. We used the mouse organotypic spinal cord cultures, ideally suited for studying long-term interference with cues delivered at controlled times and concentrations. In cultured spinal segments, the normal presence, distribution and maturation of anatomically distinct classes of neurons and resident neuroglial cells are preserved. Organotypic explants were developed for two weeks embedded in fibrin glue alone or presenting

graphene oxide nanosheets at 10, 25 and 50 μg/mL. We addressed the impact of such treatments on premotor synaptic activity monitored by patch clamp recordings of ventral interneurons. We investigated by immunofluorescence and confocal microscopy the accompanying glial responses to graphene oxide exposure, focusing on resident microglia, tested in organotypic spinal slices and in isolated neuroglia cultures. Our results suggest that microglia reactivity to accumulation of graphene oxide flakes, maybe due to active phagocytosis, may trimm down synaptic activity, although in the absence of an effective activation of inflammatory response and in the absence of neuronal cell death.

1. Introduction

Graphene is a monolayer sheet of carbon atoms, tightly bound in a hexagonal honeycomb lattice. More specifically, graphene is an allotrope of carbon in the form of a two-dimensional film of sp^2 hybridized carbon atoms (Kostarelos and Novoselov, 2014; Sanchez et al., 2012), characterized by high mechanical strength and electrical conductivity, combined with optical transparency. In neurobiology, graphene has been used in surface engineering of regenerative scaffolds to control the neuro-induction of stem cells (Wang et al., 2012), and in that of neurological interfaces to improve electrode performance (Kostarelos and Novoselov, 2014; Li et al., 2013; Mao et al., 2013; Wang et al., 2011).

Graphene oxide (GO) is the most common derivative of graphene. Recently, GO materials have been successfully designed for drug delivery applications (Liu et al. 2013; Yang et al., 2008, 2011; Baldrighi et al., 2016; Rauti et al., 2018). However, their potential persistence in biological tissues requires investigating their safety. We have previously (Rauti et al., 2016) reported the ability of small GO (< 200 nm; s-GO) nanosheets to reduce synaptic activity at glutamatergic synapses without affecting cultured hippocampal neurons survival. To date, only few studies addressed the interaction between s-GO nanosheets and synapses (Bramini et al., 2016; Rauti et al., 2016), while there are scarcely any data on the interactions between neural circuit function, s-GO tissue accumulation and inflammation. Before any further exploitation of s-GO in synaptic targeting, a detailed analysis of tissue responses to s-GO exposure is needed.

Mechanistic studies of the interplay between s-GO, the activation of microglia and synaptic function, may require *in vitro* models to interrogate central nervous system (CNS) responses at cellular resolution. Organotypic slices are explant cultures that preserve key, structural elements of the tissue of origin (Avossa et al., 2003, 2006; Fischer et al., 1998; Furlan et al., 2007; Hailer et al., 1996; Medelin et al., 2016; Schermer and Humpel, 2002; Tscherter et al., 2001) allowing detailed studies of cellular and subcellular responses, such as inflammatory reactivity and synaptic efficacy (Medelin et al., 2018), upon chronic treatments, including the exposure to exogenous factors. In the CNS, the immune response is mediated by resident macrophages called microglia that are approximately 12 % of the total CNS cells originating from myeloid cells. This subpopulation of brain cells can switch between two different phenotypes: a ramified phenotype, typical of the resting state, during which they “monitor” the surrounding environment (Cherry et al., 2014; Davalos et al., 2005; Nimmerjahn et al., 2005) and an amoeboid phenotype, which is induced by antigen-mediated stimulation. When activated, microglia rapidly changes its surface receptor expression and the

production of molecules involved in the immune response, like cytokines and chemokines (Fetler and Amigorena, 2005; Nimmerjahn et al., 2005). Activated microglia may represent an active player in neuron damage (Block et al., 2007).

We used mouse spinal organotypic cultures to mimic a chronic accumulation of s-GO in the spinal cord tissue. The s-GO nanosheets were delivered to the spinal tissue upon dilution in the chicken plasma (fibrin glue) used to embed the explants for culturing, thus allowing s-GO to rapidly adsorb proteins (Bertrand et al., 2017), to mimic how nanosheets behave in a complex biological milieu. We patch-clamped ventral interneurons to monitor synaptic transmission. Contextually, using confocal microscopy we explored the effects of s-GO on innate immunity, in both organotypic slices and primary isolated microglial cultures. We conclude that chronic accumulation of s-GO, due to localisation of high doses of the material, significantly affected synaptic activity and the microglia cell population. Our experiments in isolated microglial cells in culture support the direct response of these cells to s-GO in these experimental conditions, however in organptypic cultures we did not detect strong indicators of a switch toward the pro-inflammatory phenotype.

2. Materials and Methods

2.1 Preparation of s-GO

Synthesis and characterization of s-GO used in the present study were fully described in a separate article (Rodrigues et al., 2018). Briefly, 0.8 g of graphite flakes (Graflake 9580, Nacional Grafite Ltda., Brazil) were oxidized after mixing with 0.4 g of sodium nitrate (Merck-Sigma, UK) and 18.4 mL of sulfuric acid 99.999% (Merck-Sigma, UK), followed by 2.4 g of potassium permanganate (Merck-Sigma, UK), according to the modified Hummers method, which was described in our previous work (Ali-Boucetta et al., 2013; Rauti et al., 2016). After mixing for 30 min, 37.5 mL of water for injections (Fresenius Kabi Ltd., UK) were added dropwise to ensure the safety of the exothermic reaction taking place. The reaction temperature was further increased to 98 °C, and maintained for another 30 min. The reaction was terminated after adding 112.5 mL of water for injections, followed by the dropwise addition of 12.5 mL of hydrogen peroxide 30% (Merck-Sigma, UK). The resulting mixture was purified by several rounds of centrifugation at 9000 rpm for 20 min, until the supernatant reached a neutral pH and a viscous orange/brown layer of pure GO appeared on top of the pelleted oxidation byproducts (Jasim et al., 2016; Rauti et al., 2016). GO was exfoliated using warm water for injections and purified by centrifugation at 4000 rpm for 20 min to remove any residual graphitic impurities. The obtained GO dispersion was aliquoted to depyrogenated glass vials, which were exposed to a water bath sonicator (VWR, UK) operating at 80 W (45 kHz) for 5 min. The sonicated dispersion was then centrifuged at 13000 rpm for 5 min, and the supernatant was collected yielding s-GO nanosheets. All procedures were conducted under endotoxin-free conditions, which were attained by setting the reaction under a laminar flow hood, using depyrogenated glassware and nonpyrogenic plastic containers (Mukherjee et al., 2016).

Atomic force microscopy (AFM) images of s-GO were acquired using a Multimode 8 microscope (Bruker, UK), operating in tapping mode using OTESPA tips (Bruker, UK). Twenty µl of s-GO, diluted to a concentration of 100 µg/mL, were deposited on top of a freshly prepared mica surface

(Agar Scientific, UK) coated with poly-L-lysine (Sigma-Aldrich, UK), and dried overnight at 37 ^{o}C prior to analysis. Full physicochemical characterization of s-GO is summarized in Figure S1.

2.2 Preparation of spinal tissue slices and primary glial cultures

Organotypic cultures were obtained from spinal cords isolated from E12 embryonic mouse (C57Bl), as previously described (Avossa et al., 2003; Furlan et al., 2005, 2007; Usmani et al., 2016). Briefly, pregnant mice were sacrificed by CO_2 overdose and decapitation and fetuses delivered by caesarean section. Isolated fetuses were decapitated and their backs were isolated from low thoracic and high lumbar regions and transversely sliced (275 μm) with a tissue chopper. Cultures were fixed on a glass coverslip (Kindler, EU) with fibrin glue, i.e. reconstituted chicken plasma (Rockland) clotted with thrombin (Merk). In graphene-treated cultures, s-GO (Rauti et al., 2016) nanosheets were embedded in the fibrin glue at 10, 25 and 50 μg/mL final concentration. The distribution of s-GO within this matrix was detected via confocal microscopy under reflection mode (see below; and Patskovsky et al., 2015). Figure S2 shows the dispersion of s-GO at the different concentrations. Experiments were performed on control and s-GO treated cultures after 2 and 3 weeks *in vitro*.

All experiments were performed in accordance with the UE guidelines (Directive 2010/63/UE) and Italian law (decree 26/14) and were approved by the local authority veterinary service and by our institution (SISSA-ISAS) ethical committee. All efforts were made to minimize animal suffering and to reduce the number of animal used. Animal use was approved by the Italian Ministry of Health, in agreement with the EU Recommendation 2007/526/CE.

Primary brain glial cultures were obtained from P2−P3 rats (Wistar) cortices, as previously described (Calegari et al., 1999; Rauti et al., 2016). Dissociated cells were plated into plastic 75 cm^2 flasks, incubated (37 °C; 5% CO_2) in culture medium consisting of DMEM (Invitrogen), supplemented with 10% FBS, 100 IU/ mL penicillin, and 10 mg/mL streptomycin.

Confluent mixed glial cultures from *days in vitro* (DIV) 21 to DIV 25 were treated with a trypsin solution (0.25% trypsin, 1 mM EDTA in HBSS) diluted 1:4 in PBS for 30 minutes at 37 °C and 5% CO_2. The medium was then collected and diluted 1:4 in DMEM supplemented with 10% FBS and centrifuged for 5 minutes at 200 x g. The pellet was then re-suspended in DMEM supplemented with 10% FBS and mixed glial cultures conditioned medium (50:50) and plated on poly-L-lysine-coated glass coverslips. Twenty-four hours after trypsinization half of the cultures were incubated with s-GO at a concentration of 10 μg/mL suspended in the culture medium for 1 or 5 days.

All procedures were approved by the local veterinary authorities and performed in accordance with the Italian law (decree 26/14) and the UE guidelines (2007/526/CE and 2010/63/UE). The animal use was approved by the Italian Ministry of Health. All efforts were made to minimize suffering and to reduce the number of animals used.

2.3 Electrophysiological recordings

For patch-clamp recordings (whole-cell, voltage clamp mode), a coverslip with the spinal culture was positioned in a recording chamber, mounted on an inverted microscope (Eclipse TE-200, Nikon, Japan) and superfused with control physiological saline solution containing (in mM): 152 NaCl, 4

KCl, 1 $MgCl_2$, 2 $CaCl_2$, 10 HEPES and 10 Glucose. The pH was adjusted to 7.4 with NaOH (osmolarity 305 mosmol L^{-1}). Cells were patched with glass pipettes (4-7 MΩ) filled with a solution of the following composition (in mM): 120 Kgluconate, 20 KCl, 10 HEPES, 10 EGTA, 2 $MgCl_2$ and Na_2ATP. The pH was adjusted to 7.3 with KOH (295 mosmol L^{-1}). All electrophysiological recordings were performed at room temperature (RT; 20-22 °C) and the spontaneous synaptic activity was recorded by clamping the membrane voltage at –56 mV (not corrected for liquid junction potential, which was –14 mV). Recordings were performed from ventrally located spinal interneurons identified on the basis of previously reported criteria (Ballerini et al., 1999; Ballerini and Galante, 1998; Galante et al., 2000). We detected no differences between controls (n = 45) and s-GO (n = 39) neurons in cell membrane capacitance (70 ± 8 pF controls, 68 ± 6 pF s-GO) and membrane input resistance (250 ± 28 MΩ controls, 242 ± 20 MΩ s-GO). Spontaneous activity was also recorded in the presence of 6-cyano-7-nitroquinoxaline-2,3-dione (CNQX, 10 μM), bicuculline (20 μM) and strychnine (10 μM) to pharmacologically discriminate between glutamatergic and GABAergic PSCs, respectively. To detect miniature post-synaptic currents (mPSCs), TTX (1 μM; Latoxan, Valence, France) was added. All reagents were purchased from Sigma-Aldrich, if not otherwise indicated. Data were collected by Multiclamp 700B patch amplifier (Axon CNS, Molecular Devices) and digitized at 10 kHz with the pClamp 10.2 software (Molecular Devices LLC, USA). All recorded events were analyzed offline with the AxoGraph 1.4.4 (Axon Instrument) event detection software (Axon CNS, Molecular Devices).

2.4 Immunofluorescence labelling of spinal cord slices

Organotypic cultures were fixed by 4% formaldehyde (prepared from fresh paraformaldehyde; Sigma) in PBS for 1 hour at RT and then washed in PBS. Free aldehyde groups were quenched in 0.1 M glycine in PBS for 5 min. The samples were blocked and permeabilized in 3 % fetal bovine serum (FBS), 3 % BSA and 0.3 % Triton-X 100 in PBS for 1 h at RT. Samples were incubated with primary antibodies (mouse anti-neurofilament H Smi 32, Biolegend, 1:250 dilution; mouse monoclonal anti-GFAP, Invitrogen, 1:500 dilution; rabbit monoclonal anti-caspase 3, Euroclone, 1: 200 dilution; rabbit polyclonal anti-β-tubulin III, Sigma-Aldrich, 1:250 dilution; rabbit anti Iba1, Wako, 1:250 dilution) diluted in PBS with 5 % FBS at 4 °C, overnight. Samples were then incubated in secondary antibodies (Alexa 488 goat anti-mouse, Invitrogen, 1:500 dilution; Alexa 594 goat anti-rabbit, Invitrogen, 1:500 dilution), and DAPI (Invitrogen, dilution 1:200) to stain the nuclei, for 2 h at RT and finally mounted on 1 mm glass coverslips using Vectashield hardset mounting medium (Vector Laboratories). Images were acquired using a Nikon C2 Confocal, equipped with Ar/Kr, He/Ne and UV lasers. Images were acquired with a 40× (1.4 NA) or 60× (1.5 NA) oil-objective (using oil mounting medium, 1.515 refractive index). Confocal sections were acquired every 500 nm and the total Z-stack thickness (50 μm) was set such that all emitted fluorescence was collected from the sample. Regions of interest were confined to the ventral part of slice. Offline analysis was performed using the open source image-processing package Fiji (Schindelin et al., 2012) and Volocity software (Volocity 3D image analysis software, PerkinElmer, USA).

2.5 Immunofluorescence labelling of neuroglia primary cultures

Primary glial and microglial cultures were fixed by 4 % formaldehyde (prepared from fresh paraformaldehyde) in PBS for 20 min at RT and then washed in PBS. Free aldehyde groups were quenched in 0.1 M glycine in PBS for 5 min. The samples were blocked and permeabilized in 5 % fetal bovine serum (FBS), 0.3 % Triton-X 100 in PBS for 30 min at RT. Samples were incubated with primary antibodies (mouse monoclonal anti-GFAP, Invitrogen, 1:500 dilution; rabbit anti Iba1, Wako, 1:250 dilution; mouse monoclonal anti-Brdu, Thermo Fisher, 1:200 dilution) diluted in PBS with 5 % FBS at 4 °C, overnight. Samples were then incubated in secondary antibodies (Alexa 488 goat anti-mouse, Invitrogen, 1:500 dilution; Alexa 594 goat anti-rabbit, Invitrogen, 1:500 dilution), and DAPI (Invitrogen, dilution 1:200) to stain the nuclei, for 45 minutes at RT and finally mounted on 1 mm thick glass coverslips using Vectashield mounting medium (Vector Laboratories). Cells densities were quantified at 20× (0.5 NA) magnification using a DM6000 Leica microscope (Leica Microsystems GmbH, Wetzlar, Germany). In order to investigate the internalization of s-GO in microglial cells, we used the reflection mode property during the confocal acquisition. Images were acquired using a Nikon C2 Confocal, equipped with Ar/Kr, He/Ne and UV lasers. Images were acquired with a 40× (1.4 NA) oil-objective (using oil mounting medium, 1.515 refractive index). Confocal sections were acquired every 200 nm and the total Z-stack thickness 20µm.

2.6 Bromodeoxyuridine (BrdU) incorporation

Microglial primary cultures were incubated with BrdU (Thermo Fisher) diluted in the culture medium at a final concentration of 10 µM for 24 hours. Cells were then washed with PBS and fixed by 4 % formaldehyde (prepared from fresh paraformaldehyde) for 20 minutes at RT and then washed with PBS (3 times, 2 minutes each). Free aldehyde groups were quenched in 0.1 M glycine in PBS for 5 min. Cells were then incubated with HCl 1 M for 1 minutes on ice and with HCl 2 M for 15 minutes at 37 °C. Acid was then neutralized with boric acid 0.1 M for 10 minutes at RT. The samples were then blocked and permeabilized in 3 % fetal bovine serum (FBS) and 0.3 % Triton-X 100 in PBS for 1h at RT. Samples were incubated with primary antibodies at 4 °C overnight (mouse monoclonal anti-BrdU, 1:200 dilution; rabbit anti-Iba1, 1:200 dilution). Samples were then incubated in secondary antibodies (Alexa 488 goat anti-mouse, Invitrogen, 1:500 dilution; Alexa 594 goat anti-rabbit, Invitrogen, 1:500 dilution), and DAPI (Invitrogen, dilution 1:200) to stain the nuclei, for 45 minutes at RT and mounted on 1 mm thick glass coverslips using Vectashield mounting medium (Vector Laboratories).

2.7 Microvesicle isolation

Microvesicles shedding and detection by western blotting were performed as previously described (Rauti et al., 2016). Microvesicles release was induced in 21 DIV microglial cells by the stimulation with benzoyl-ATP (bzATP; 100 µM) in saline solution with the following composition: 125 mM NaCl, 5 mM KCl, 1.2 mM $MgSO_4$, 1.2 mM KH_2PO_4, 2 mM $CaCl_2$, 6 mM D-glucose, and 25 mM HEPES/NaOH (pH adjusted to 7.4), for 30 min at 37 °C and 5% CO_2. Microvesicles were then pelleted by centrifugation (Bianco et al., 2009). Negative controls were incubated with saline solution without the presence of bzATP. MVs were re-suspended in lysis buffer (50 mM Tris-HCl, pH 8.0, 150 mM NaCl, 1 % NP40, 0.1 % SDS), sonicated 3 × 10 s, and then boiled at 95 °C for 5 min.

Samples were run on a 10 % polyacrylamide gel and were blotted onto nitrocellulose filters (Millipore, Italy). Filters were then blocked in PBS-Tween-20 (0.1 %) plus 5 % nonfat dry milk and incubated with the primary antibody antiflotillin-1 (dilution 1:1000) for 16 h at 4 °C. Specific MV marker flotillin-1 (Al-Nedawi et al., 2008; del Conde et al., 2005) was detected with mouse monoclonal antiflotillin-1 (dilution 1:1000). After three washes with PBS-Tween, filters were incubated with peroxidase-conjugated anti-mouse secondary antibody (dilution 1:1000). Optical density of immunolabeled ECL-exposed protein bands was measured with UVI-1D software.

2.8 Microglial morphological analysis

For morphological analysis cells were fixed and immunostained for Iba1 and DAPI for nuclei, as described above and images were acquired with a 40 × oil objective. The quantitative analysis of cell morphology was performed with the particle analysis feature in Fiji (1.51v) to automatically measure the area, perimeter and Feret's maximum diameter. In particular, Feret's diameter is described as the greatest distance between any two points along cell perimeter and is considered as an index of cell length (Caldeira et al., 2014; Kurpius et al., 2006; Mitchell et al., 2018; Torres-Platas et al., 2014; Zanier et al., 2015). A more ramified cell has a higher value for this parameter, while a more amoeboid shape is described by a lower value. We also evaluated the transformation index (Caldeira et al., 2014; Fujita et al., 1996) which is calculated as [perimeter of cell (μm)]^2/4π [cell area (μm^2)] and describes the degree of cellular ramification. Cells with long processes and small cell body display larger values of the transformation index, which depends on the cell shape regardless the cell size.

2.9 Measurement of cytokines and chemokines

In a small set of experiments an inflammatory response was induced (Hanisch, 2002), by incubating organotypic slices, for 6 hours, with a cocktail of the following mouse recombinant cytokines: TNF-α (R&D Systems, #210-TA/CF), IL-1β (R&D Systems, #M15330), GM-CSF (R&D Systems, #P04141), 10 ng/mL each, or with lipopolysaccharide (LPS, 1 ng/mL). Inflammatory reaction may be detected by cytokine and chemokine production. A panel of 12 out of cytokines or chemokines was measured in organotypic culture supernatants after 2 weeks culturing, by Luminex based technology, using a customized Procarta plex Immunoassay kit (Invitrogen), following the manufacturer's protocol. The following soluble factors were simultaneously measured in 50 µl of supernatant: IL4, IL6, IL10, IL17, IL21, BAFF, IFNγ, TNFα, CXCL1, CXCL2, CXCL10, MCP1.

2.10 Statistical Analysis

The results are presented as the mean ± SD, if not otherwise indicated. Statistically significant difference between two data sets was assessed by t-statistic, in particular by Student's *t*-test (after checking variances homogeneity by Leven's test) for parametric data and by Mann-Whitney's test for non-parametric ones (Statistica 6.0 – StatSoft Italy). Differences among multiple groups were evaluated by F-statistic with two-way ANOVA, followed by the Holm-Sidak test for multiple comparison (Sigmaplot 12.0 – Systat Software).

A statistically significant difference between two data sets was assessed and $P < 0.05$ was considered statistically significant.

In box-plots, the thick horizontal bar indicates the median value, the cross indicates the mean value, the boxed area extends from the 25^{th} to 75^{th} percentiles while whiskers from the 5^{th} to the 95^{th} percentiles.

3. Results

3.1 Long-Term Exposure to High Doses of s-GO Impaired Network Activity in Spinal-Cord Organotypic Slices. We first explored the long-term (2 weeks) exposure of neural tissue to s-GO in 3D tissue cultures. s-GO was delivered to the neural tissue *via* the fibrin glue, the thick matrix obtained by chicken plasma and thrombin in which slices are embedded (see Methods), that represents the explant growth environment. Figure 1A shows a reconstruction at low confocal magnification of a spinal cord slice after 14 days of growth, labelled for neurofilament H (Smi-32; in green) and for the nuclei (DAPI, in blue). The entire area of tissue growth is visualized, and it includes the spinal slice, at the centre, and the outgrowing area comprising the co-cultured dorsal root ganglia (DRG) and the typical, dense mesh of Smi-32^+ neurites in the surrounding outgrowth belt (Fabbro et al., 2012).

Spinal organotypic slices upon 2 weeks of culturing exhibit an intense spontaneous synaptic activity (Ballerini and Galante, 1998; Furlan et al., 2007; Streit, 1993). We patch clamped (sketched in Figure 1B) visually identified ventral interneurons (at holding potential, V_h of – 56 mV) in control cultures (n = 45) and in s-GO treated ones (n = 52), and we recorded spontaneous, basal postsynaptic currents (PSCs). Figure 1C shows representative tracings in control (top) and after exposure to the highest dose (50 μg/mL) of s-GO (bottom). In all culture groups, PSCs appeared as heterogeneous inward currents of variable amplitudes, characterized by different kinetic properties (fast decaying events, with decay time constant (τ) of 6 ± 2 ms and slow decaying events with τ 22 ± 6, n = 15, see sample in Figure 1C, right panel; Medelin et al., 2018).

The chronic (2 weeks) exposure to low (10 μg/mL) doses of s-GO did not affect PSCs amplitude and frequency values (39 ± 7 pA and 23 ± 5 Hz, n = 13) when compared to control ones (42 ± 6 pA and 24 ± 4 Hz, n = 15; plots in Figure 1D). Conversely, higher s-GO doses significantly (25 and 50 μg/mL, $P < 0.05$ and $P < 0.01$, respectively; two-way ANOVA) reduced PSCs frequency (from 24 ± 6 Hz in control to 14 ± 3 Hz, in s-GO 25 μg/mL, n = 15 and 13; from control 22 ± 8 Hz to 10 ± 2 Hz in s-GO 50 μg/mL, n = 15 and 13; plot in Figure 1D, left). Upon s-GO treatments, PSCs decay kinetics (fast decaying, τ 5 ± 2 ms and slow decaying τ 26 ± 3, n = 13 at 50 μg/mL, see sample Figure 1C bottom row, right) and amplitudes were not altered by these treatments (Figure 1D, right). In 25 and 50 μg/mL s-GO treated cultures we investigated the amount of neuronal apoptosis in respect to aged-matched controls by measuring the expression of active caspase-3 (Cohen, 1997). Active caspase-3 positive cells were quantified in the ventral spinal horns (Figure 1E, in red). We detected a comparative amount of apoptotic cells in all conditions (in control: 15 ± 3 Caspase-3 positive cells/mm^2 namely 3.7 % of the total amount of cells, n = 10 visual fields and in s-GO 50 μg/mL; 20 ± 3 Caspase-3 positive cells/mm^2, 4.3 % of the cells, n = 10 visual fields; plot in Figure 1E). Thus, s-GO only when delivered at higher concentrations altered synapse function, without increasing neuronal cell death.

Miniature synaptic currents (mPSCs; Figure 2) were recorded in a subset of control (n = 12) and s-GO treated (n = 13) neurons by application of tetrodotoxin (TTX, 1 μM), to block voltage-gated sodium channels. As this treatment impairs the generation of action potentials, mPSCs reflect the stochastic release of vesicles from the presynaptic terminals at individual synapses impinging onto the recorded neuron. Their frequency depends on the pre-synaptic release probability and on the number of synaptic contacts, while their amplitude depends on postsynaptic receptor sensitivity (Raastad et al., 1992). In neurons exposed to low (10 μg/mL) s-GO, mPSCs frequency was not affected (from 19 ± 3 Hz in control to 15 ± 3 Hz in s-GO treated slices; plot in Figure 2). When investigating the impact of higher graphene doses (25 and 50 μg/mL), we detected a significant difference ($P < 0.05$ and $P < 0.01$, respectively; two-way ANOVA) in mPSCs frequency (from 20 ± 3 Hz to 13 ± 2 Hz in s-GO 25μg/mL and from 16 ± 3 Hz to 6 ± 1 Hz in s-GO 50 μg/mL). s-GO did not affect the amplitude of the recorded events (from 27 ± 6 pA in controls to 32 ± 5 pA in s-GO 10 μg/mL; from 29 ± 5 pA in controls to 27 ± 4 pA in s-GO 25 μg/mL; from 33 ± 8 pA in controls to 30 ± 6 pA in s-GO 50 μg/mL).

In s-GO neurons (50 μg/mL) we pharmacologically (see Methods) isolated AMPA-receptor mediated glutamatergic mEPSCs (n = 13) or $GABA_A$- receptor mediated mIPSCs (n = 13), both detected as inward currents in our recording conditions (Medelin et al., 2016). mEPSCs and mIPSCs frequency values were similarly reduced by s-GO when compared to control slices (for mEPSPs in controls 14 ± 4 Hz, n = 12; in s-GO 7 ± 2 Hz, n = 13; $P < 0.05$, Student's *t* test; histograms in Figure 2, bottom-left panel; for mIPSCs in controls 13 ± 4 Hz, n = 12; in s-GO 5 ± 2 Hz, n = 13; $P < 0.05$, Student's *t* test; histograms in Figure 2, bottom-right panel).

3.2 s-GO Exposure at High Doses Induced Microglial Proliferation. To investigate tissue reactivity accompanying s-GO ability to alter synaptic signalling, we used the highest dose tested, namely the s-GO at 50 μg/mL. In organotypic slice cultures, neuroglia resident cells are mainly represented by astrocytes (GFAP positive cells) and microglia (Iba1 positive cells; Medelin et al., 2018).

GFAP-positive astrocytes are not immune cells *per se*, but can, under certain conditions, contribute to the immune response (Farina et al., 2007). In organotypic cultures upon 2 weeks of culturing, these cells are usually characterized by a stellate-like morphology (Figure 3A; Avossa et al., 2003) and their density was not significantly altered by s-GO treatment (Figure 3A, right histograms; 500 ± 70 GFAP-positive cells/mm^2 in control and 650 ± 90 GFAP-positive cells in s-GO; n = 13 visual fields each). Iba1-positive microglia cells are known mediators of CNS inflammation. In contrast to astrocytes, the density of Iba1-positive cells was significantly ($P < 0.01$, Student's *t* test) increased in slices exposed to s-GO (47 ± 17 Iba1-positive cells/mm^2, n = 10 fields in control and 150 ± 30 Iba1-positive cells/mm^2, n = 11 fields for s-GO; Figure 3B).

To further investigate glia cell reactivity to s-GO treatment in complex systems, we measured from the spinal cord cultures supernatant (n = 6 slices for each conditions) the presence of cytokine and chemokine after 2 weeks of continuous exposure. In s-GO we detected an increased trend of expression, when compared to controls, of CXCL2, and MCP1, T lymphocytes and monocytes recall factors, and IL6, IL10, BAFF and TNFα, cytokines responsible for pro-inflammatory responses (IL6, TNFα), regulatory function (IL10) and homeostatic B cell survival (BAFF), however the profiles of

soluble factors production obtained from our analysis, did not reach statistical significance (Figure 3C). These observations are in line with a limited or even absent sustained activation of microglial cells toward both polarized forms: M1 and M2, or most probably toward an intermediate one (Kabba et al., 2018).

3.3 s-GO Exposure Induces Microglial Proliferation in Neuroglial Cultures. The increased density of microglial cell in the absence of significant increased production and release of chemokines and cytokines after 2 weeks exposure to high s-GO dose, prompted us to directly investigate the effects of s-GO on microglial cell types in isolated glial preparations, obtained from early post-natal rats (P2-P3). Due to the relatively low-cell density typical of cultures comprising isolated Iba1-positive cells, as shown in Figure 4A (control), we exposed the cells for 5 days to a lower (10 μg/mL) dose of s-GO. s-GO readily increased Iba1-positive cell-density, as shown in Figure 4A, a response reminiscent of the one observed in organotypic slices (Figure 3B). In order to assess whether s-GO sheets induced microglia reactivity, we analysed the cellular shape, a traditionally accepted index of the phenotypes microglia acquires when entrained in tissue responses. In particular, a highly ramified shape is linked to a surveillant state in which microglia actively monitors the surrounding environment. On the other hand, an amoeboid phenotype may indicate the transition to the activated, pro-inflammatory state (Saijo and Glass, 2011). Consistent with a transformation from a ramified to an amoeboid phenotype, the perimeter, Feret's maximum diameter and transformation index (plot in Figure 4B), significantly decreased ($P_{perimeter}<0.0001$, $P_{Feret's\ diameter}=0.0035$, $P_{transformation\ index}<0.0001$; Mann-Whitney test) after 6 days of s-GO exposure, compared to control (n = 10 visual fields for both conditions; 3 different cultures series). The measured parameters reliably describe morphological changes and cell length. In particular, the Feret's maximum diameter is defined as the highest distance between any two points along the cell perimeter while transformation index describes cellular ramification.

Next, we analysed the number of cycling cells present in each culture group (control and s-GO). For this purpose, cells were pulsed at 24 h and at 5 days with 10 mM bromodeoxyuridine (BrdU) prior to fixation. The number of cells that had incorporated the nucleotide analogue was then assessed by immunofluorescence, using anti-BrdU-specific antibodies. In Figure 4C the box plot shows the $BrdU^+/Iba1^+$ ratio, an index of microglial cells that incorporated BrdU in the newly synthesized DNA during cell division, providing a quantitative measure of proliferative capacity of cells (Nowakowski et al., 1989). The higher $BrdU^+/Iba1^+$ ratio was already significant at 24 hours of s-GO exposure ($median_{GO}= 0.85$; $median_{control}=0.08$), suggesting an early interaction of microglia with small graphene sheets. The increased proliferation was more pronounced after five days of incubation with s-GO ($median_{GO}= 0.2$; $median_{control}=0.45$; $P < 0.001$, Mann-Whitney test, for both time points; n=10 fields for each condition; 4 different cultures).

Microvesicles (MVs), released from almost all cell brain types, are, in general, an emerging intercellular communication over long-range distance. In particular, MVs discharged by microglial cells represent a secretory pathway for inflammatory cytokine (Turola et al., 2012) potentially promoting propagation of neuroinflammatory responses in the brain. We measured the release of MVs from isolated microglial cultures in control or exposed to s-GO by western blot analysis for the protein flotillin-1, a marker of lipid rafts that are specific plasma membrane regions were the

probability of MVs release is higher (Figure 4D; Rauti et al., 2016). Pharmacological stimulation by bzATP induces only a slight release of MVs in isolated microglial cells, as depicted by the particularly weak signal in the specific band (Figure 4D). Interestingly, bzATP stimulation in the presence of s-GO triggers a massive microglia shedding of MVs, shown by the high intensity of the band (Figure 4D).

3.4 Localization of s-GO in microglial cells. We then directly investigated the fate of s-GO in isolated microglia cultures using confocal microscopy reconstructions. Iba1-positive cells (2 different culture series) were exposed for 3 days to s-GO (10 μg/mL). We tested the presence of s-GO sheets within Iba1 positive cells by operating the confocal microscopy under reflection mode, which allows the visualization of s-GO (Jung et al., 2007; Kim et al., 2010; Bramini et al., 2016; Chiacchiaretta et al., 2018). Figure 5A shows confocal reconstructions of control and treated Iba1 positive cells. In s-GO-treated cells, GO nano-sheet aggregates (in yellow, reflection mode) were detected inside microglial cells (in grey, $Iba1^{+}$) by z-stack reconstruction (Figure 5, top panels: 40 ×; 100 × 100 μm^2 visualized area). In Figure 5, high magnification confocal micrographs (control and s-GO treated, bottom panels) are shown (60 ×; 50 × 50 μm^2 visualized area) depicting a single microglia (grey) cell co-localisation with the reflected signal of graphene (yellow). The orthogonal view of the z-projection shows the XZ and YZ planes (bottom side and right side of the z-stack reconstructed image, respectively) of the acquired fields. As expected from cells that act as macrophages, the material were internalized and stocked inside the cell, forming small aggregates, appreciable by the orthogonal reconstruction. The signal of s-GO was not present in control cells, either in the z-stack reconstruction or in the orthogonal planes (Figure 5, left panels).

4. Discussion

We used here organotypic spinal cord cultures to test tissue responses to s-GO prolonged exposure. In particular, we were interested in assessing microglia reactivity in cultured neural explants, where immune resident cells are present, but not supported by the peripheral ones. Organotypic spinal slices represent a biological model of segmental spinal microcircuit useful for studying the dynamics of intrasegmental processes. A long series of studies has indicated that the organotypic cultures from mouse spinal cord represent a valuable *in vitro* model system to study the mechanisms of development, neurogenesis, glial differentiation, myelination, muscle formation, and synaptogenesis leading to early post natal features, upon 2 weeks of culturing (Avossa et al., 2003; Rosato-Siri et al., 2004; Fabbro et al., 2007; Sibilla et al., 2009; Furlan et al., 2007; Medelin et al., 2016). More recently, we confirmed the presence of heterogeneous neuroglial cells after 2 weeks of *in vitro* growth and we further documented in organotypic spinal tissue the induction, by short-term incubation with pro-inflammaotry CKs cocktail, of a reliable release of cytokines and chemokines, mostly due to the local generation and delivery of inflammatory factors (Medelin et al., 2018). Thus, our experimental model is ideally suited to dissect spinal resident cells ability in modulating local inflammatory tissue reactivity.

The major result of the present investigation is that the long-term accumulation of s-GO (when delivered at high doses) affected resident microglia and, in the absence of an effective clearance, may induce a subtle, although chronic, reactive state, potentially trimming down synaptic activity, as physiologically occurring during development (Paolicelli et al., 2011). In fact, in our experiments, both GABAR- and AMPAR-mediated mPSCs were reduced in frequency upon s-GO exposure at high concentrations. The reduction in miniatures' frequency, but not in their amplitude, strongly suggests a reduction in the number of synapses or of release sites (Rauti et al., 2016). This down-regulation of synapses is apparently not due to a general cell membrane disruption or to neuronal apoptosis. In fact, we never detected alterations in basic electrophysiological parameters, reflecting neuronal health and membrane integrity (Carp, 1992; Djuric et al., 2015). This indicated, together with the absence of up-regulated apoptosis that the synaptic events diminished not as a consequence of direct neuronal damage brought about by s-GO.

In organotypic slices, both glutamate- and GABA-mediated synapses were down-regulated by s-GO, this result differs from our previous report, where s-GO down-regulated selectively glutamatergic release sites in hippocampal cultures (Rauti et al., 2016). Considering the similarity of the s-GO batch used here compared to our previous study (Figure S1), the lack of specific synaptic targeting may be related to several factors, such as the diverse CNS regions tested, i.e. ventral spinal cord *vs* hippocampus, the initially more immature stage of network and synapse development (embryonic *vs* postnatal) or the s-GO higher concentrations. In this context, it is relevant to note the s-GO delivery modality used here: s-GO was accumulated in the fibrin glue embedding the spinal culture and, presumably, was from here released along 2 weeks of culturing. Thus the potential formation of a protein corona might have affected the nanoparticle biological fate (Hadjidemetriou et al., 2015) favouring active phagocytosis by neuroglia and preventing the direct synapse interference described in our previous report (Rauti et al., 2016). It is temptive to speculate that the presence in the spinal explants of resident neuroglia resulted in active phagocytosis restricted to intrinsic microglia, without the involvement of blood cells such as macrophages. Such an activation could have induced a generic microglia response, known as synaptic stripping, ultimately leading to indiscriminate synapse reduction (Kettenmann et al., 2013).

In spinal organotypic slices exposed to s-GO, the presence of tissue reactivity is indicated only by the observed increase in microglia cell-density, in the absence of increased GFAP+ astrocytes, suggesting only a mild state of reactivity (Liddelow et al., 2017; Okada et al., 2018; Olson, 2010). Interestingly, the cytokines and chemokines profiles measured in organotypic cultures supernatant, although slightly altered, were not significantly increased after 2 weeks of s-GO exposure. In this regard, we did not found an increase in IL-6, that is produced by astrocyte following, for example, a proinflammatory stimulation (Ulivieri et al., 2016). Therefore, in this model, we may hypothesize that microglial proliferative response with no significant variation in cytokines production after 2 weeks, does not involve a shift into the M1 phenotype.

The results in this study obtained with isolated $Iba1^+$ cells are in support of a direct activation of microglial cells as a consequence of active s-GO phagocytosis. s-GO boosted microglia proliferation leading to a significantly higher cell density in pure neuroglia cultures, accompanied by the typical morphological switch from a ramified to an amoeboid phenotype (Cherry et al., 2014; Kettenmann et al., 2011; Nimmerjahn et al., 2005; Saijo and Glass, 2011), suggestive of an active

role of Iba1-positive cells in the tissue reaction to graphene, even in the virtual absence of other cell types. The direct activation of microglia was apparently related to fast internalization of s-GO flake aggregates that occurs during the first 24h after the exposure.

We thus suggest that s-GO, accumulated via the fibrin glue, activates resident microglia phagocytosis. This hypothesis is also supported by the observation that pure microglial cultures grown and exposed to s-GO in a serum-free medium did not show a proliferation boost comparable to that found in the presence of FBS (Figure S3). As already discussed above, the interaction of nanoparticles such as s-GO with biological fluids may affect their fate and effectiveness. In fact, the corona formation takes place not only in the presence of plasma proteins like fibrinogen but also with proteins present in the serum (Gräfe et al., 2016). Therefore, the proliferative response found in both pure microglial cultures and organotypic slices exposed to s-GO, despite their different origin and architecture, may be explained by an increase of the efficacy in the uptake of the material (Walkey et al., 2012) by microglia and mediated by s-GO interactions with the proteins pool of plasma and serum.

An additional indication of microglia reactivity in s-GO was provided by the increased release of shed vesicles induced by bzATP. MVs released by microglia have been reported to affect synaptic activity, mainly acting at the presynaptic site of the excitatory synapses, but increasing synaptic activity and glutamate release in primary cultures (Antonucci et al., 2012) thus it seems unfeasible that the down-regulation in synaptic activity detected in this study be mediated by MVs release.

One possibility is that, in the current experimental conditions, the global reduction in synaptic activity is mostly due to the emergence of chronic, although mild, tissue reactivity. Such reactivity follows microglia phagocytic activity of protein-decorated s-GO flakes. Ultimately, we have to ask ourselves whether these data indicate a potential in vivo inflammatory response due to s-GO sheets. There are several relevant aspects that limit reporting it as an inflammatory response. First of all, the conditions we tested involved the delivering of s-GO to a “closed” biological system, allowing only resident macrophages to interact with it and limiting the contribution of neighbour tissues in the interaction with this material, as it would happen in an in vivo model. The lack of significance in the chemokine and cytokine increase in concentration suggests a mild immune response that may not necessarily lead to a pathological inflammatory state or alternatively indicates a return to a physiological condition, from an intermediate immune activation. Last, astrocytes, which depend on microglia activation to be polarized to pro-inflammatory cells did not show, in this context, reactive gliosis. To note, a recent report (Song et al., 2014) investigated microglia pro- and/or anti-inflammatory responses when challenged by different graphene structures, and documented anti-inflammatory effects of 3D-graphene foams.

Microglia produces immune mediators secondary to neuronal stimulation, (i.e. tissue injury), or following a direct stimulus to microglia itself. Here we report an increased proliferation rate of Iba1-positive cells, suggestive of microglia activation, and consistent with morphological observations. However, the detected cell activation seems to involve a group of cells, not all of them, and this may explain the fact that we observed only a trend toward increased production of immune factors, without significant variations. We may hypothesize that the fraction of activated microglia includes cells in direct contact to s-GO. Indeed, microglia is often reported to function similarly to

other myeloid cells, the macrophages, able to scavenge the environment, perform phagocytosis, antigen presentation and to react to contact with nano materials (Aldinucci et al., 2013; Jin and Yamashita, 2016) in order to maintain CNS homeostasis, with both detrimental and beneficial effects. It is important to underline that eventually the pro-inflammatory molecules, present before and after s-GO contact, were not inducing astrogliosis. Therefore, as a side effect, our in vitro model allows the direct observation and study of material/neuron interactions in the presence of glial cells, and also simulates accumulation of material in CNS providing useful insights on the potential consequences.

The function of microglia, brain macrophages, is still poorly understood. In mice there are at least two subtypes: inflammatory and non-classical patrolling cells (Nimmerjahn et al., 2005), and also a CNS region-dependent microglial heterogeneity has been suggested, suggesting that microglia, although in many different ways, is constantly activated. In this complex picture, we were interested in investigating whether s-GO induced an inflammatory reaction. Our results indicate that this was not the case. Further studies should indeed address the interplay between microglia and s-GO, for example by single cell RNA sequencing (Matcovitch-Natan et al., 2016), a method that has sufficient sensibility to determine the functional/phenotypic response of these important brain-macrophage cell population.

5. Figures

Figure 1. s-GO reduced basal synaptic activity in a dose-response fashion without inducing cell death in organotypic ventral horns. In (A), low magnification confocal micrograph of a spinal cord slice culture (14 DIV) immune-labelled for neurofilament H (SMI-32; in green) and nuclei (DAPI; in blue). Scale bar 500 μm. The arrow head indicates the ventral fissure, localizing the ventral horns, while the arrows the co-cultured DRGs. In (B), sketch of the experimental setting for ventral interneuron single cell recordings (modified with permission from Usmani et al., 2016). In (C), tracings represent spontaneous synaptic activity recorded from ventral interneurons in Control (top) and s-GO treated slices (bottom; 50 μg/mL). On the right panel, isolated fast and slow PSCs are shown superimposed (electronic average trace superimposed in white) for the control (top) and s-GO treated (bottom) recordings (same cells as above). In (D), the plots summarize the average PSCs frequency (left) and amplitude (right) values; note the reduction in PSC frequency upon s-GO treatments (25 and 50 μg/mL) (* $P < 0.05$ and ** $P < 0.01$). In (E), confocal micrographs visualize caspase-3 positive cells (in red) in the ventral horns, counter-stained for β-tubulin III (in green, to visualize neurons) in Control (left) and s-GO (50 μg/mL; right) treated slices. Nuclei are visualized by DAPI (blue). Scale bar: 50 μm. The column plot summarizes the density of caspase and β-tubulin double positive cells; note the absence of statistical significant differences between the two conditions.

Figure 2. Miniature synaptic currents are down regulated by s-GO in organotypic ventral horns. Sample tracings are mPSCs recorded in Control and s-GO (50 μg/mL) treated cultures (top left panel). Top right: plot reporting mPSCs frequency values in control and in the three different s-GO concentrations tested. Note that s-GO treatments (25 and 50 μg/mL) significantly decreased the frequency of mPSCs (* $P < 0.05$ and ** $P < 0.01$). Bottom: column plots summarize the average values of AMPA-glutamate (left; mEPSCs) and $GABA_A$ (right, mIPSCs) receptor mediated miniature events, pharmacologically isolated. In s-GO treatments (50 μg/mL) a significant decrease in the frequency of both types of miniature was detected (* $P < 0.05$ and ** $P < 0.01$, respectively).

Figure 3. Tissue reactivity in organotypic spinal cultures exposed to s-GO at high dose. In (A), GFAP immune-labelling to visualize astrocytes in Control and s-GO treated slices (50 μg/mL). Both cultures were labelled for GFAP (in green) and nuclei (DAPI; in blue) Scale bar 100 μm. Note that the GFAP+ cell density did not differ between the two conditions (column plot). In (B), immunofluorescence images are shown to visualize glial and microglial cells in Control and s-GO (50 μg/mL) treated slices (anti-Iba1, in red; anti-GFAP in green; DAPI in blue). Scale bar 50 μm. Note that Iba1+ cell density was significantly (** $P < 0.01$) increased by s-GO (50 μg/mL; right column plot). (C), Plots summarize the Milliplex assay measures to assess the production of the following cytokines in organotypic culture supernatant: IL6, IL10, TNF and BAFF and chemokines: CXCL1, CXCL2, CXCL10 and MCP1 in the presence or absence of s-GO, after 2 weeks *in vitro*. Column graphs report mean values ± SEM of 5 independent experiments.

Figure 4. Increased cell reactivity in pure microglia cell cultures exposed to s-GO. In (A), immunofluorescence micrographs visualize microglia by Iba1 labelling (in red) in Control and s-GO treated cultures (10 μg/mL). Scale bar 50 μm. The column graph summarizes microglial density in the two conditions. Note that Iba1+ cell density is significantly (*** $P < 0.001$) higher in cultures treated by s-GO. In (B), high magnification confocal micrographs of Iba1+ cells highlight their morphology in the two conditions. The right column plots summarizes perimeter, Ferret's maximum diameter and transformation index, parameters that describe cellular ramification. All of them are significantly reduced after s-GO exposure (***$P_{perimeter} < 0.0001$, **$P_{Feret's\ diameter} < 0.001$, ***$P_{transformation\ index} < 0.0001$; Mann-Whitney test).
In (C), box plots show the brdU+/Iba1+ ratio measured in isolated microglial cultures 24 h and 5 days after s-GO exposure (10 μg/mL) (*** $P < 0.001$). In (D), western blot analysis of the MVs marker flotillin-1 in each condition. Microvesicles were isolated from glial cultures incubated with s-GO (10 μg/mL) for 6 days and then treated or not with bzATP.

Figure 5. s-GO activates microglia phagocytosis in pure neuroglia cultures. Representative confocal reconstruction of microglial cells in Control or s-GO (10 μg/mL) treated cultures. Scale bar 20 μm. In the bottom panel, for both conditions a 60 × zoom (50 × 50 μm field) of a single microglial cell is shown. Scale bar 20 μm. Cultures are immunostained for Iba1 (in grey), and DAPI (in blue), s-GO is visualized by the reflection mode of the confocal system (in yellow). s-GO sheets are visible as aggregates coloured in yellow inside the cell.

6 Conflict of Interest

The authors declare that the research was conducted in the absence of any commercial or financial relationships that could be construed as a potential conflict of interest.

7 Author Contributions

M.M. and R.R. performed all cell biology, electrophysiology, and confocal experiments and analysis; A.F.R. and K.K. contributed to the synthesis and characterization of thin graphene oxide (s-GO); E.B. and C.B. designed and performed the supernatant measures; C.B. and L.B. conceived the study and the experimental design; C.B., R.R. and L.B. wrote the manuscript.

8 Funding

We acknowledged financial support from the European Union's Horizon 2020 research and innovation programme under grant agreement No. 696656 and No. 785219 Graphene Flagship.

9 Acknowledgments

We are especially grateful to Gabriele Baj for the confocal reconstructions of microglial cells generated at the Light Microscopy Imaging Center (LMIC) of the University of Trieste - Life Sciences Department. We are indebt with Dr Neus Lozano for her help in providing the intial s-GO.

10 References

Al-Nedawi, K., Meehan, B., Micallef, J., Lhotak, V., May, L., Guha, A., et al. (2008). Intercellular transfer of the oncogenic receptor EGFRvIII by microvesicles derived from tumour cells. *Nat. Cell Biol.* 10, 619–624. doi:10.1038/ncb1725.

Aldinucci, A., Turco, A., Biagioli, T., Toma, F. M., Bani, D., Guasti, D., et al. (2013). Carbon Nanotube Scaffolds Instruct Human Dendritic Cells: Modulating Immune Responses by Contacts at the Nanoscale. *Nano Lett.* 13, 6098–6105. doi:10.1021/nl403396e.

Ali-Boucetta, H., Bitounis, D., Raveendran-Nair, R., Servant, A., Van den Bossche, J., and Kostarelos, K. (2013). Purified Graphene Oxide Dispersions Lack In Vitro Cytotoxicity and In Vivo Pathogenicity. *Adv. Healthc. Mater.* 2, 433–441. doi:10.1002/adhm.201200248.

Antonucci, F., Turola, E., Riganti, L., Caleo, M., Gabrielli, M., Perrotta, C., et al. (2012). Microvesicles released from microglia stimulate synaptic activity via enhanced sphingolipid metabolism. *EMBO J.* 31, 1231–40. doi:10.1038/emboj.2011.489.

Avossa, D., Grandolfo, M., Mazzarol, F., Zatta, M., and Ballerini, L. (2006). Early signs of motoneuron vulnerability in a disease model system: Characterization of transverse slice cultures of spinal cord isolated from embryonic ALS mice. *Neuroscience* 138, 1179–1194. doi:10.1016/j.neuroscience.2005.12.009.

Avossa, D., Rosato-Siri, M. D., Mazzarol, F., and Ballerini, L. (2003). Spinal circuits formation: a study of developmentally regulated markers in organotypic cultures of embryonic mouse spinal cord. *Neuroscience* 122, 391–405.

Baldrighi, M., Trusel, M., Tonini, R., and Giordani, S. (2016). Carbon Nanomaterials Interfacing with Neurons: An In vivo Perspective. *Front. Neurosci.* 10, 250. doi:10.3389/fnins.2016.00250.

Ballerini, L., and Galante, M. (1998). Network bursting by organotypic spinal slice cultures in the presence of bicuculline and/or strychnine is developmentally regulated. *Eur. J. Neurosci.* 10, 2871–9.

Ballerini, L., Galante, M., Grandolfo, M., and Nistri, A. (1999). Generation of rhythmic patterns of activity by ventral interneurones in rat organotypic spinal slice culture. *J. Physiol.* 517 (Pt 2), 459–75. doi:10.1111/J.1469-7793.1999.0459T.X.

Bertrand, N., Grenier, P., Mahmoudi, M., Lima, E. M., Appel, E. A., Dormont, F., et al. (2017). Mechanistic understanding of in vivo protein corona formation on polymeric nanoparticles and impact on pharmacokinetics. *Nat. Commun.* 8, 777. doi:10.1038/s41467-017-00600-w.

Bianco, F., Perrotta, C., Novellino, L., Francolini, M., Riganti, L., Menna, E., et al. (2009). Acid sphingomyelinase activity triggers microparticle release from glial cells. *EMBO J.* 28, 1043–54. doi:10.1038/emboj.2009.45.

Block, M. L., Zecca, L., and Hong, J. S. (2007). Microglia-mediated neurotoxicity: uncovering the molecular mechanisms. *Nat. Rev. Neurosci.* 8, 57–69. doi:10.1038/nrn2038.

Bramini, M., Sacchetti, S., Armirotti, A., Rocchi, A., Vázquez, E., León Castellanos, V., et al.

(2016). Graphene Oxide Nanosheets Disrupt Lipid Composition, Ca $^{2+}$ Homeostasis, and Synaptic Transmission in Primary Cortical Neurons. *ACS Nano* 10, 7154–7171. doi:10.1021/acsnano.6b03438.

Calegari, F., Coco, S., Taverna, E., Bassetti, M., Verderio, C., Corradi, N., et al. (1999). A regulated secretory pathway in cultured hippocampal astrocytes. *J. Biol. Chem.* 274, 22539–47.

Caldeira, C., Oliveira, A. F., Cunha, C., Vaz, A. R., Falcão, A. S., Fernandes, A., et al. (2014). Microglia change from a reactive to an age-like phenotype with the time in culture. *Front. Cell. Neurosci.* 8, 152. doi:10.3389/fncel.2014.00152.

Carp, J. S. (1992). Physiological properties of primate lumbar motoneurons. *J. Neurophysiol.* 68, 1121–32. doi:10.1152/jn.1992.68.4.1121.

Cherry, J. D., Olschowka, J. A., and O'Banion, M. (2014). Neuroinflammation and M2 microglia: the good, the bad, and the inflamed. *J. Neuroinflammation* 11, 98. doi:10.1186/1742-2094-11-98.

Chiacchiaretta, M., Bramini, M., Rocchi, A., Armirotti, A., Giordano, E., Vázquez, E., Bandiera, T., Ferroni, S., Cesca, F., Benfenati, F. (2018). Graphene oxide upregulates the homeostatic functions of primary astrocytes and modulates astrocyte-to-neuron communication. *Nano Lett.* doi: 10.1021/acs.nanolett.8b02487

Cohen, G. M. (1997). Caspases: the executioners of apoptosis. *Biochem J*. 326, 1-16

Davalos, D., Grutzendler, J., Yang, G., Kim, J. V, Zuo, Y., Jung, S., et al. (2005). ATP mediates rapid microglial response to local brain injury in vivo. *Nat. Neurosci.* 8, 752–758. doi:10.1038/nn1472.

del Conde, I., Shrimpton, C. N., Thiagarajan, P., and López, J. A. (2005). Tissue-factor-bearing microvesicles arise from lipid rafts and fuse with activated platelets to initiate coagulation. *Blood* 106, 1604–1611. doi:10.1182/blood-2004-03-1095.

Djuric, U., Cheung, A. Y. L., Zhang, W., Mok, R. S., Lai, W., Piekna, A., et al. (2015). MECP2e1 isoform mutation affects the form and function of neurons derived from Rett syndrome patient iPS cells. *Neurobiol. Dis.* 76, 37–45. doi:10.1016/j.nbd.2015.01.001.

Fabbro, A., Bosi, S., Ballerini, L., and Prato, M. (2012). Carbon Nanotubes: Artificial Nanomaterials to Engineer Single Neurons and Neuronal Networks. *ACS Chem. Neurosci.* 3, 611–618. doi:10.1021/cn300048q.

Fabbro, A., Pastore, B., Nistri, A., Ballerini, L. (2007). Activity-independent intracellular Ca^{2+} oscillations are spontaneously generated by ventral spinal neurons during development in vitro. *Cell Calcium* 41, 317-329. doi: 10.1016/j.ceca.2006.07.006

Farina, C., Aloisi, F., and Meinl, E. (2007). Astrocytes are active players in cerebral innate immunity. *Trends Immunol.* 28, 138–145. doi:10.1016/j.it.2007.01.005.

Fetler, L., and Amigorena, S. (2005). NEUROSCIENCE: Brain Under Surveillance: The Microglia Patrol. *Science (80).* 309, 392–393. doi:10.1126/science.1114852.

689 Fischer, H. P., Marksteiner, J., Ransmayr, G., Saria, A., and Humpel, C. (1998). NGF but not GDNF
690 or neurturin enhance acetylcholine tissue levels in striatal organotypic brain slices. *Int. J. Dev.*
691 *Neurosci.* 16, 391–401.

692 Fujita, H., Tanaka, J., Toku, K., Tateishi, N., Suzuki, Y., Matsuda, S., et al. (1996). Effects of GM-
693 CSF and ordinary supplements on the ramification of microglia in culture: a morphometrical
694 study. *Glia* 18, 269–81.

695 Furlan, F., Guasti, L., Avossa, D., Becchetti, A., Cilia, E., Ballerini, L., et al. (2005). Interneurons
696 transiently express the ERG K+ channels during development of mouse spinal networks in vitro.
697 *Neuroscience* 135, 1179–1192. doi:10.1016/j.neuroscience.2005.06.040.

698 Furlan, F., Taccola, G., Grandolfo, M., Guasti, L., Arcangeli, A., Nistri, A., et al. (2007). ERG
699 Conductance Expression Modulates the Excitability of Ventral Horn GABAergic Interneurons
700 That Control Rhythmic Oscillations in the Developing Mouse Spinal Cord. *J. Neurosci.* 27,
701 919–928. doi:10.1523/JNEUROSCI.4035-06.2007.

702 Galante, M., Nistri, A., and Ballerini, L. (2000). Opposite changes in synaptic activity of organotypic
703 rat spinal cord cultures after chronic block of AMPA/kainate or glycine and GABAA receptors.
704 *J. Physiol.* 523 Pt 3, 639–51. doi:10.1111/J.1469-7793.2000.T01-1-00639.X.

705 Gräfe, C., Weidner, A., Lühe, M. v.d., Bergemann, C., Schacher, F. H., Clement, J. H., et al. (2016).
706 Intentional formation of a protein corona on nanoparticles: Serum concentration affects protein
707 corona mass, surface charge, and nanoparticle–cell interaction. *Int. J. Biochem. Cell Biol.* 75,
708 196–202. doi:10.1016/j.biocel.2015.11.005.

709 Hadjidemetriou, M., Al-Ahmady, Z., Mazza, M., Collins, R. F., Dawson, K., and Kostarelos, K.
710 (2015). *In Vivo* Biomolecule Corona around Blood-Circulating, Clinically Used and Antibody-
711 Targeted Lipid Bilayer Nanoscale Vesicles. *ACS Nano* 9, 8142–8156.
712 doi:10.1021/acsnano.5b03300.

713 Hailer, N. P., Jarhult, J. D., and Nitsch, R. (1996). Resting microglial cells in vitro: analysis of
714 morphology and adhesion molecule expression in organotypic hippocampal slice cultures. *Glia*
715 18, 319–31.

716 Hanisch, U.-K. (2002). Microglia as a source and target of cytokines. *Glia* 40, 140–155.
717 doi:10.1002/glia.10161.

718 Jasim, D. A., Lozano, N., and Kostarelos, K. (2016). Synthesis of few-layered, high-purity graphene
719 oxide sheets from different graphite sources for biology. *2D Mater.* 3, 014006.
720 doi:10.1088/2053-1583/3/1/014006.

721 Jin, X., and Yamashita, T. (2016). Microglia in central nervous system repair after injury. *J.*
722 *Biochem.* 159, 491–496. doi:10.1093/jb/mvw009.

723 Jung, I., Pelton, M., Piner, R., Dikin, D. A., Stankovich, S., Watcharotone, S., Hausner, M., Ruoff, R.
724 S. (2007). Simple approach for high-contrast optical imaging and characterization of graphene-
725 based sheets. *Nano Lett*. 7, 3569–3575. doi: 10.1021/nl0714177

726 Kabba, J. A., Xu, Y., Christian, H., Ruan, W., Chenai, K., Xiang, Y., et al. (2018). Microglia:

Housekeeper of the Central Nervous System. *Cell. Mol. Neurobiol.* 38, 53–71. doi:10.1007/s10571-017-0504-2.

Kettenmann, H., Hanisch, U.-K., Noda, M., and Verkhratsky, A. (2011). Physiology of Microglia. *Physiol. Rev.* 91, 461–553. doi:10.1152/physrev.00011.2010.

Kettenmann, H., Kirchhoff, F., and Verkhratsky, A. (2013). Microglia: New Roles for the Synaptic Stripper. *Neuron* 77, 10–18. doi:10.1016/j.neuron.2012.12.023.

Kim, J., Kim, F., Huang, J. (2010). Seeing graphene-based sheets. *Materials Today* 13, 28-38. doi:10.1016/S1369-7021(10)70031-6

Kostarelos, K., and Novoselov, K. S. (2014). Exploring the Interface of Graphene and Biology. *Science (80-.).* 344, 261–263. doi:10.1126/science.1246736.

Kurpius, D., Wilson, N., Fuller, L., Hoffman, A., and Dailey, M. E. (2006). Early activation, motility, and homing of neonatal microglia to injured neurons does not require protein synthesis. *Glia* 54, 58–70. doi:10.1002/glia.20355.

Li, N., Zhang, Q., Gao, S., Song, Q., Huang, R., Wang, L., et al. (2013). Three-dimensional graphene foam as a biocompatible and conductive scaffold for neural stem cells. *Sci. Rep.* 3, 1604. doi:10.1038/srep01604.

Liddelow, S. A., Guttenplan, K. A., Clarke, L. E., Bennett, F. C., Bohlen, C. J., Schirmer, L., et al. (2017). Neurotoxic reactive astrocytes are induced by activated microglia. *Nature* 541, 481–487. doi:10.1038/nature21029.

Liu, J., Cui, L., and Losic, D. (2013). Graphene and graphene oxide as new nanocarriers for drug delivery applications. Acta Biomater. 9, 9243–9257. doi:10.1016/J.ACTBIO.2013.08.016.

Mao, H. Y., Laurent, S., Chen, W., Akhavan, O., Imani, M., Ashkarran, A. A., et al. (2013). Graphene: Promises, Facts, Opportunities, and Challenges in Nanomedicine. *Chem. Rev.* 113, 3407–3424. doi:10.1021/cr300335p.

Matcovitch-Natan, O., Winter, D. R., Giladi, A., Vargas Aguilar, S., Spinrad, A., Sarrazin, S., et al., (2016). Microglia development follows a stepwise program to regulate brain homeostasis. *Science*. 353, aad8670. doi: 10.1126/science.aad8670.

Medelin, M., Giacco, V., Aldinucci, A., Castronovo, G., Bonechi, E., Sibilla, A., et al. (2018). Bridging pro-inflammatory signals, synaptic transmission and protection in spinal explants in vitro. *Mol. Brain* 11, 3. doi:10.1186/s13041-018-0347-x.

Medelin, M., Rancic, V., Cellot, G., Laishram, J., Veeraraghavan, P., Rossi, C., et al. (2016). Altered development in GABA co-release shapes glycinergic synaptic currents in cultured spinal slices of the SOD1 ^{G93A} mouse model of amyotrophic lateral sclerosis. *J. Physiol.* 594, 3827–3840. doi:10.1113/JP272382.

Mitchell, D. M., Lovel, A. G., and Stenkamp, D. L. (2018). Dynamic changes in microglial and macrophage characteristics during degeneration and regeneration of the zebrafish retina. *J. Neuroinflammation* 15, 163. doi:10.1186/s12974-018-1185-6.

Mukherjee, S. P., Lozano, N., Kucki, M., Del Rio-Castillo, A. E., Newman, L., Vázquez, E., et al. (2016). Detection of Endotoxin Contamination of Graphene Based Materials Using the TNF-α Expression Test and Guidelines for Endotoxin-Free Graphene Oxide Production. *PLoS One* 11, e0166816. doi:10.1371/journal.pone.0166816.

Nimmerjahn, A., Kirchhoff, F., and Helmchen, F. (2005). Resting Microglial Cells Are Highly Dynamic Surveillants of Brain Parenchyma in Vivo. *Science (80-.).* 308, 1314–1318. doi:10.1126/science.1110647.

Nowakowski, R. S., Lewin, S. B., and Miller, M. W. (1989). Bromodeoxyuridine immunohistochemical determination of the lengths of the cell cycle and the DNA-synthetic phase for an anatomically defined population. *J. Neurocytol.* 18, 311–318. doi:10.1007/BF01190834.

Okada, S., Hara, M., Kobayakawa, K., Matsumoto, Y., and Nakashima, Y. (2018). Astrocyte reactivity and astrogliosis after spinal cord injury. *Neurosci. Res.* 126, 39–43. doi:10.1016/j.neures.2017.10.004.

Olson, J. K. (2010). Immune response by microglia in the spinal cord. *Ann. N. Y. Acad. Sci.* 1198, 271–278. doi:10.1111/j.1749-6632.2010.05536.x.

Paolicelli, R. C., Bolasco, G., Pagani, F., Maggi, L., Scianni, M., Panzanelli, P., Giustetto, M., Ferreira, T. A., Guiducci, E., Dumas, L., Ragozzino, D., Gross, C. T. (2011). Synaptic pruning by microglia is necessary for normal brain development. *Science* 333, 1456-1458. doi: 10.1126/science.1202529.

Patskovsky, S., Bergeron, E., Rioux, D., Meunier, M. (2015). Wide-field hyperspectral 3D imaging of functionalized gold nanoparticles targeting cancer cells by reflected light microscopy. *J Biophotonics* 8, 401-407. doi: 10.1002/jbio.201400025

Raastad, M., Storm, J. F., and Andersen, P. (1992). Putative Single Quantum and Single Fibre Excitatory Postsynaptic Currents Show Similar Amplitude Range and Variability in Rat Hippocampal Slices. *Eur. J. Neurosci.* 4, 113–117.

Rauti, R., Lozano, N., León, V., Scaini, D., Musto, M., Rago, I., et al. (2016). Graphene Oxide Nanosheets Reshape Synaptic Function in Cultured Brain Networks. *ACS Nano* 10. doi:10.1021/acsnano.6b00130.

Rauti, R., Musto, M., Bosi, S., Prato, M., Ballerini, L. (2018). Properties and behavior of carbon nanomaterials when interfacing neuronal cells: How far have we come? *Carbon* 143, 430-446. doi:10.1016/j.carbon.2018.11.026

Rodrigues, A. F., Newman, L., Lozano, N., Mukherjee, S. P., Fadeel, B., Bussy, C., Kostarelos, K. (2018). A blueprint for the synthesis and characterisation of thin graphene oxide with controlled lateral dimensions for biomedicine. *2D Mater*. 5, 035020. doi:10.1088/2053-1583/aac05c

Rosato-Siri, M. D., Zoccolan, D., Furlan, F., Ballerini, L. (2004). Interneurone bursts are spontaneously associated with muscle contractions only during early phases of mouse spinal network development: a study in organotypic cultures. *Eur J Neurosci*. 20, 2697-2710. doi: 10.1111/j.1460-9568.2004.03740.x

Saijo, K., and Glass, C. K. (2011). Microglial cell origin and phenotypes in health and disease. *Nat. Rev. Immunol.* 11, 775–787. doi:10.1038/nri3086.

Sanchez, V. C., Jachak, A., Hurt, R. H., and Kane, A. B. (2012). Biological Interactions of Graphene-Family Nanomaterials: An Interdisciplinary Review. *Chem. Res. Toxicol.* 25, 15–34. doi:10.1021/tx200339h.

Schermer, C., and Humpel, C. (2002). Granulocyte macrophage-colony stimulating factor activates microglia in rat cortex organotypic brain slices. *Neurosci. Lett.* 328, 180–4.

Schindelin, J., Arganda-Carreras, I., Frise, E., Kaynig, V., Longair, M., Pietzsch, T., et al. (2012). Fiji: an open-source platform for biological-image analysis. *Nat. Methods* 9, 676–682. doi:10.1038/nmeth.2019.

Sibilla, S., Fabbro, A., Grandolfo, M., D'Andrea, P., Nistri, A., Ballerini, L. (2009). The patterns of spontaneous Ca^{2+} signals generated by ventral spinal neurons in vitro show time-dependent refinement. *Eur J Neurosci*. 29, 1543-1559. doi: 10.1111/j.1460-9568.2009.06708.x.

Song, Q., Jiang, Z., Li, N., Liu, P., Liu, L., Tang, M., Cheng, G. (2014). Anti-inflammatory effects of three-dimensional graphene foams cultured with microglial cells. *Biomaterials* 35, 6930-6940. doi: 10.1016/j.biomaterials.2014.05.002

Streit, J. (1993). Regular oscillations of synaptic activity in spinal networks in vitro. *J. Neurophysiol.* 70, 871–878. doi:10.1152/jn.1993.70.3.871.

Torres-Platas, S. G., Comeau, S., Rachalski, A., Bo, G. D., Cruceanu, C., Turecki, G., et al. (2014). Morphometric characterization of microglial phenotypes in human cerebral cortex. *J. Neuroinflammation* 11, 12. doi:10.1186/1742-2094-11-12.

Tscherter, A., Heuschkel, M. O., Renaud, P., and Streit, J. (2001). Spatiotemporal characterization of rhythmic activity in rat spinal cord slice cultures. *Eur. J. Neurosci.* 14, 179–90.

Turola, E., Furlan, R., Bianco, F., Matteoli, M., and Verderio, C. (2012). Microglial microvesicle secretion and intercellular signaling. *Front. Physiol.* 3, 149. doi:10.3389/fphys.2012.00149.

Ulivieri, C., Savino, M. T., Luccarini, I., Fanigliulo, E., Aldinucci, A., Bonechi, E., Benagiano, M., Ortensi, B., Pelicci, G., D'Elios, M. M., Ballerini, C., Baldari, C. T. (2016). The adaptor protein Rai/ShcC promotes astrocyte-dependent inflammation during experimental autoimmune encephalomyelitis. *J Immunol*. 197, 480-490. doi: 10.4049/jimmunol.1502063.

Usmani, S., Aurand, E. R., Medelin, M., Fabbro, A., Scaini, D., Laishram, J., et al. (2016). 3D meshes of carbon nanotubes guide functional reconnection of segregated spinal explants. *Sci. Adv.* 2, e1600087. doi:10.1126/sciadv.1600087.

Walkey, C. D., Olsen, J. B., Guo, H., Emili, A., and Chan, W. C. W. (2012). Nanoparticle Size and Surface Chemistry Determine Serum Protein Adsorption and Macrophage Uptake. *J. Am. Chem. Soc.* 134, 2139–2147. doi:10.1021/ja2084338.

Wang, Y., Lee, W. C., Manga, K. K., Ang, P. K., Lu, J., Liu, Y. P., et al. (2012). Fluorinated Graphene for Promoting Neuro-Induction of Stem Cells. *Adv. Mater.* 24, 4285–4290.

doi:10.1002/adma.201200846.

Wang, Y., Li, Z., Wang, J., Li, J., and Lin, Y. (2011). Graphene and graphene oxide: biofunctionalization and applications in biotechnology. *Trends Biotechnol.* 29, 205–212. doi:10.1016/j.tibtech.2011.01.008.

Yang, X., Wang, Y., Huang, X., Ma, Y., Huang, Y., Yang, R., et al. (2011). Multi-functionalized graphene oxide based anticancer drug-carrier with dual-targeting function and pH-sensitivity. *J. Mater. Chem.* 21, 3448–3454. doi:10.1039/C0JM02494E.

Yang, X., Zhang, X., Liu, Z., Ma, Y., Huang, Y., and Chen, Y. (2008). High-Efficiency Loading and Controlled Release of Doxorubicin Hydrochloride on Graphene Oxide. *J. Phys. Chem. C* 112, 17554–17558. doi:10.1021/jp806751k.

Zanier, E. R., Fumagalli, S., Perego, C., Pischiutta, F., and De Simoni, M.-G. (2015). Shape descriptors of the "never resting" microglia in three different acute brain injury models in mice. *Intensive Care Med. Exp.* 3, 7. doi:10.1186/s40635-015-0039-0.

Figure 1.TIF

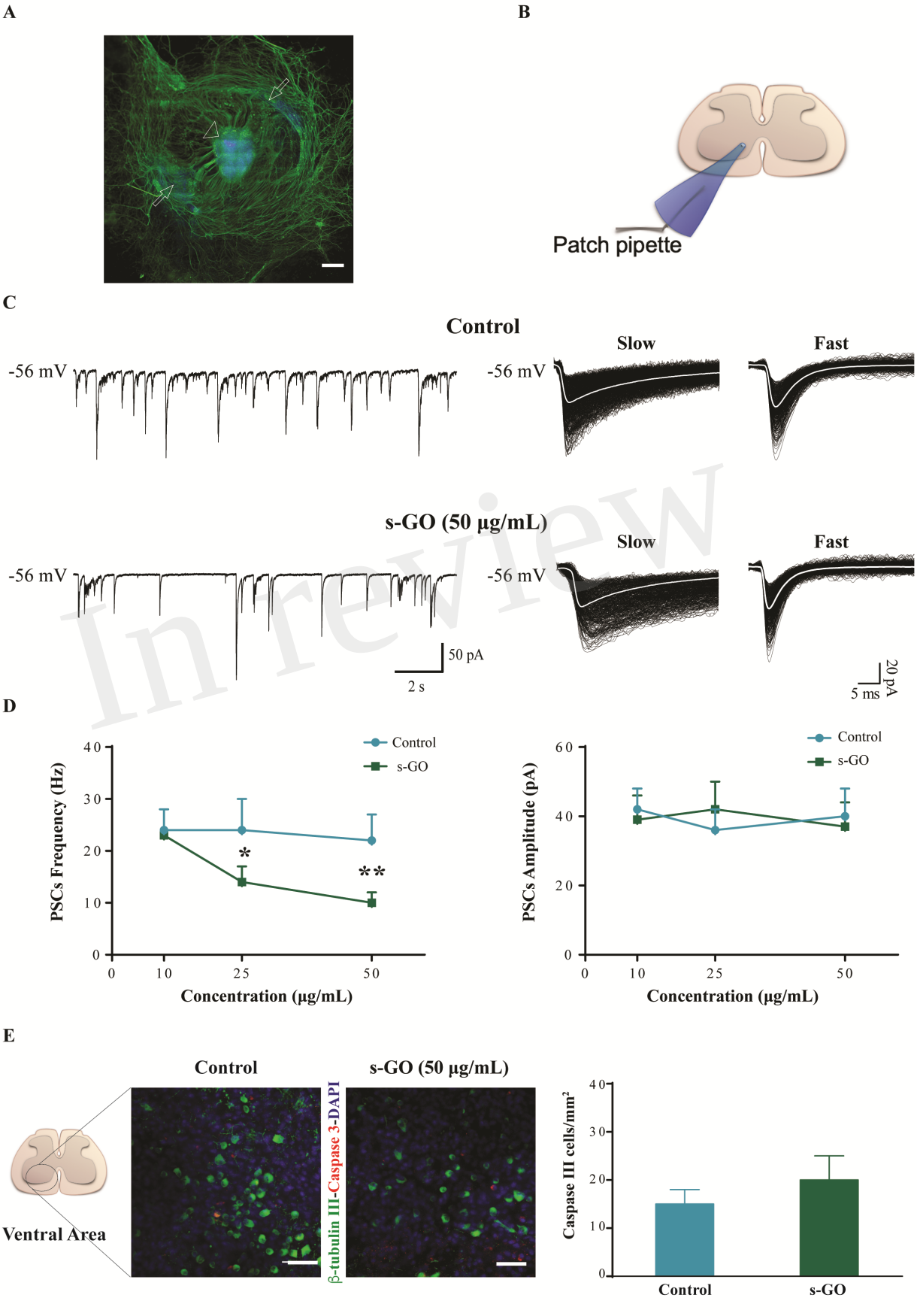

Figure 2.TIF

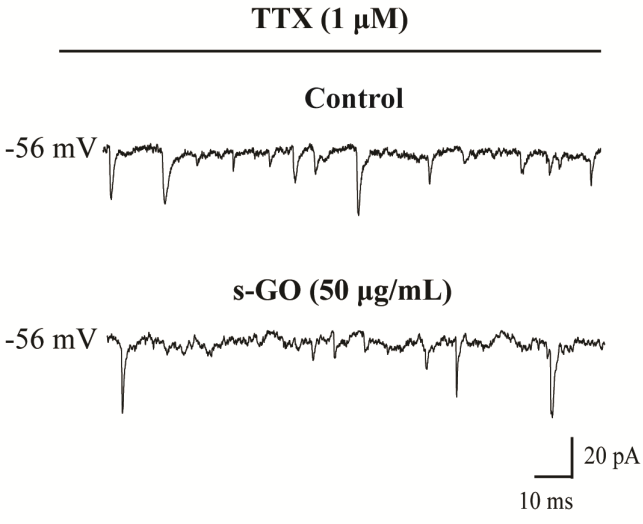

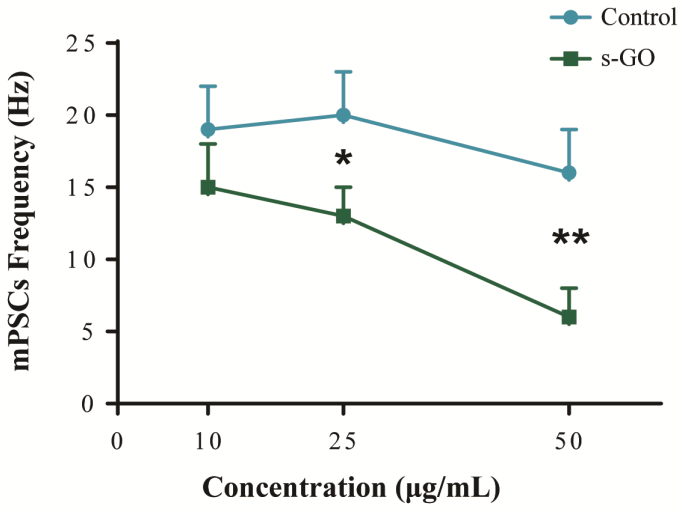

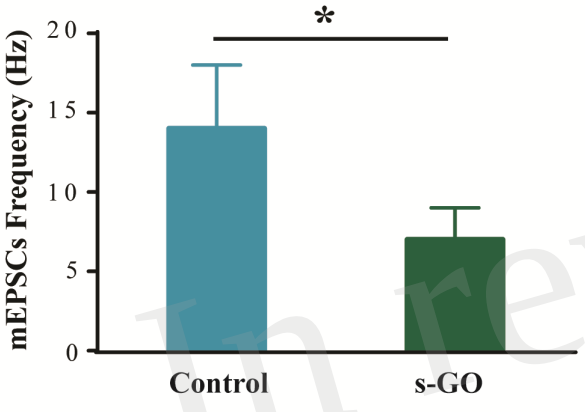

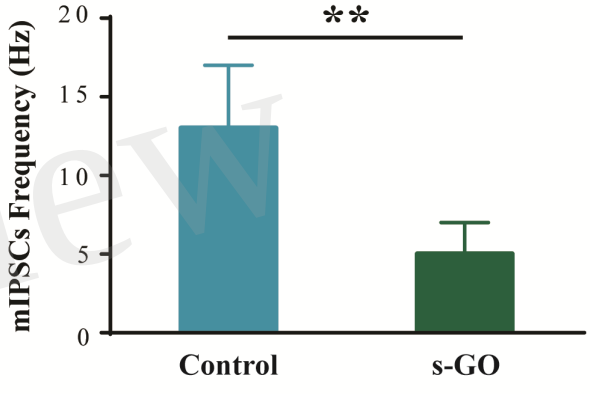

Figure 3.TIF

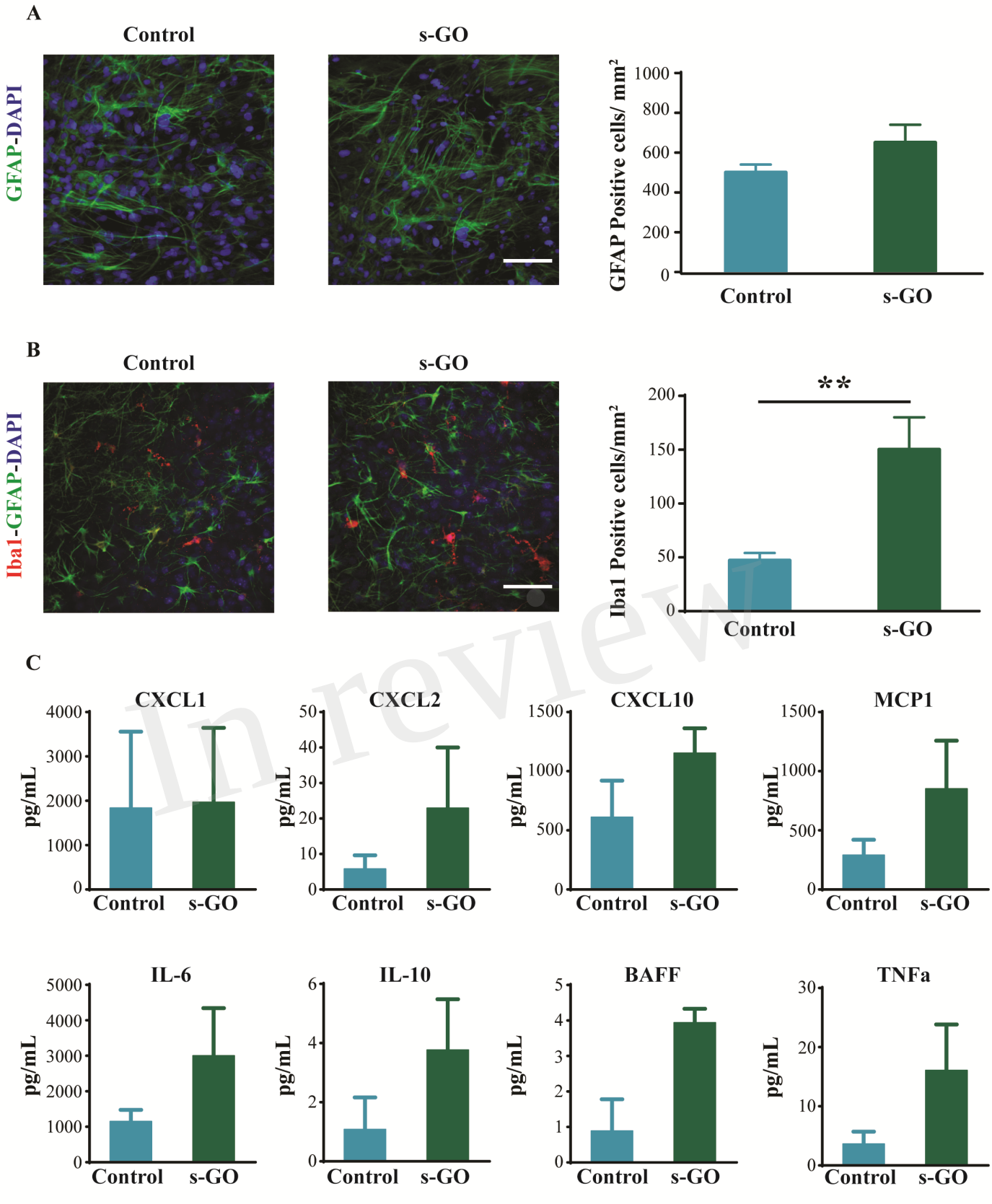

Figure 4.TIF

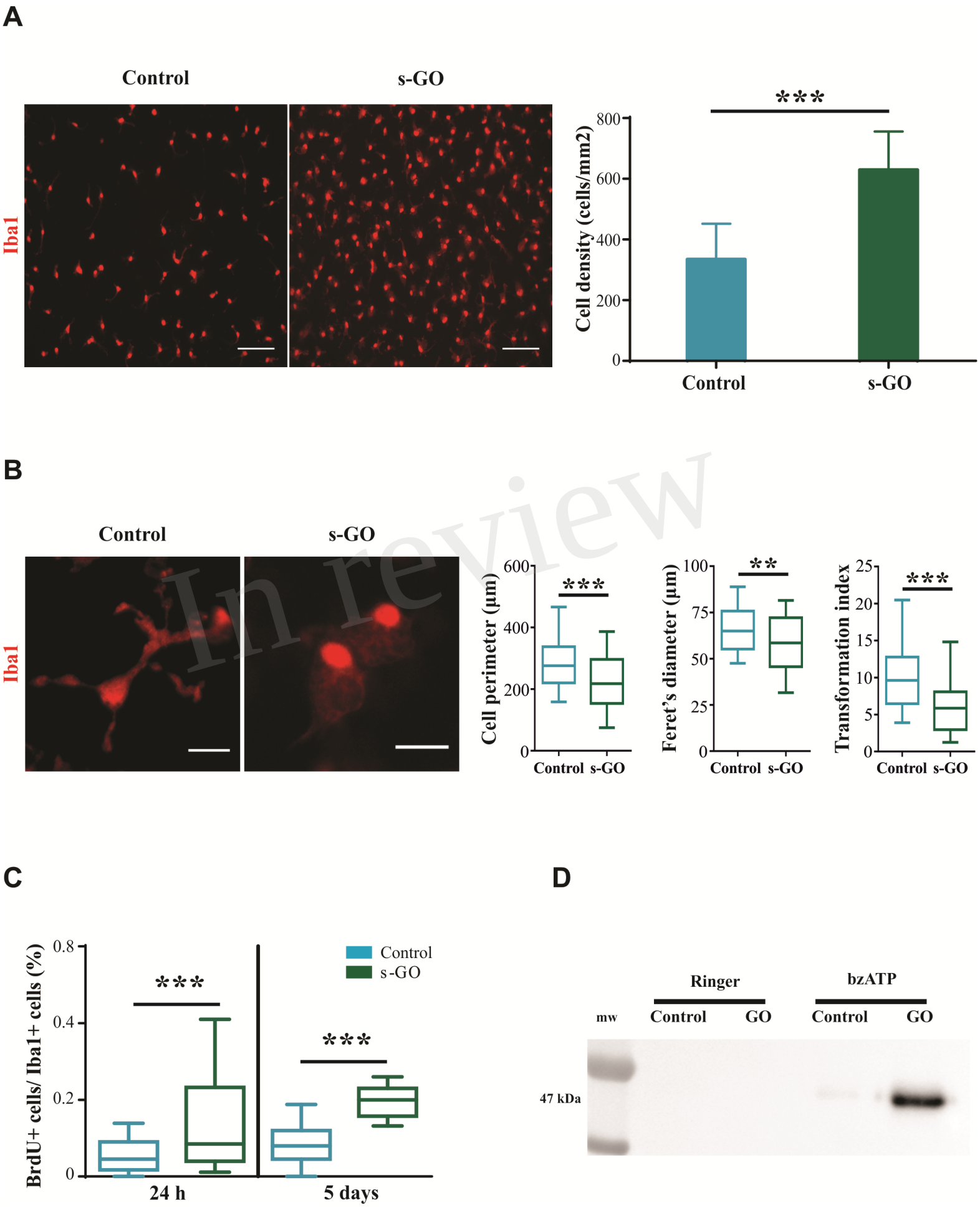

Figure 5.TIF